Emergent Simplicities in Stochastic Intergenerational Homeostasis

Kunaal Joshi[1,†], Charles S. Wright[1,†], Karl F. Ziegler[1,†], Elizabeth M. Spiers[1], Jacob T. Crosser[1], Samuel Eschker[1], Rudro R. Biswas[1*], Srividya Iyer-Biswas[1,2*]

[1]Department of Physics and Astronomy, Purdue University, West Lafayette, Indiana, USA,
[2]Santa Fe Institute, Santa Fe, NM 87501, USA.

[†]These authors contributed equally
[*]Correspondence: rrbiswas@purdue.edu, iyerbiswas@purdue.edu

Abstract

Biological systems are complex and hierarchical. Yet, key physiological "state" variables are effectively held in homeostasis despite the inherent stochasticity of constitutive molecular processes. To identify quantitative rules governing the control systems responsible for homeostasis, we reconceptualize homeostasis as a dynamical—albeit stochastic—process, rather than as an end state (i.e., a setpoint). We focus on cell size homeostasis as a valuable case study. Using our SChemostat technology, we obtain high-precision multigenerational trains of cell sizes of statistically identical, non-interacting individual *Caulobacter crescentus* cells in precisely controlled environments. Characterizing the typical generational size of a bacterium by the size immediately following a division event, we first establish that individual cells indeed maintain stochastic intergenerational size homeostasis. Through extensive data analysis from single-cell experiments under multiple growth conditions, we uncover hidden simplicities in these data, including an intergenerational scaling law governing fluctuations in cell sizes across different generations. These "emergent simplicities" comprehensively describe the dynamics—in turn they specify (without need for any fitting parameters) the precise stochastic map governing the intergenerational evolution of cell sizes. Importantly, we find that intergenerational cell size homeostasis is achieved through memory-free, reflexive elastic adaptation. Thus, under balanced growth conditions, cell size cannot serve as a repository of intergenerational memory.

Introduction

Homeostasis is a self-regulating process wherein a complex system maintains its internal stability, despite changing external conditions. This concept has played a central role in physiology since the field's inception [1]. As formulated by Bernard, stability of an organism's "internal milieu" is not simply a feature, but indeed a prerequisite for life [2]. Cannon later coined the term "homeostasis" to signify maintenance of similar (*homeo-*) and not identical (*homo-*) states, to underscore that internal parameters may vary yet successfully sustain "constancy" of key homeostatic variables within a desired tolerance [3, 4]. Thus, stochasticity in the homeostatic variable, such as that arising from the inherently probabilistic nature of the underlying biophysical dynamics, has a natural place in any realistic conceptual framework of homeostasis.

Mechanical self-regulating control systems, such as a thermostat that maintains a specified setpoint of temperature, are often used to illustrate concepts relating to homeostasis. Analogously, an organism is thought to defend the "setpoint" values of homeostatic variables [5] against intrinsic and extrinsic fluctuations. (Indeed, the mathematical language to describe feedback control in biological systems was developed alongside the concepts of cybernetics and control theory in mechanical systems [6]). Within this perspective, deviations from desired setpoints are taken to indicate organismal malfunction, with abnormal values of homeostatic variables being used to identify avenues for therapeutic interventions [7, 8].

From the systems design point of view, how do biological control systems enforce organismal homeostases? To make headway, we identify and define two distinct possibilities. One option is what we call

passive "elastic adaptation", which involves reflexive responses to instantaneous conditions with no retention of long-term memory. An organism simply senses the deviation of the current value of the homeostatic variable from the desired setpoint, and switches on the appropriate mechanism to either increase or decrease its value. The first technical model of homeostasis ever realized, Ashby's Homeostat [9], falls in to this category. Since this model lacked any "memory" and simply responded to each deviation independently of previous encounters, it was criticized as being too simplistic to capture the essence of homeostasis in natural systems. A more sophisticated control system is that of active "plastic adaptation", with past experiences stored and used to achieve reflective responses. In this scenario, a controller strategically integrates over a finite memory of past fluctuations encountered by the organism, and coordinates with a sensor that monitors the present conditions. The controller thereby learns from previous experiences to compute what anticipatory changes may be optimal, and delivers corresponding instructions to the lower layers of organismal organization (such as those governed by underlying genetic networks). An early technical model of plastic homeostasis was implemented by Shannon [10] to directly address the criticism directed toward Ashby's Homeostat: his "Maze Solving Machine" stored memories of trajectories from past excursions, which a "sensing finger" used to circumvent dead ends. These two paradigms correspond to distinct mechanisms for achieving and sustaining homeostasis. Which scheme(s) do organisms use? Is stochastic homeostasis a reactive process that does not biophysically store memories of the past or is it a memoryful, complex, and adaptive process with exquisitely controlled memory integrators?

Biological systems have layered architectures and hierarchical organization, which must somehow conspire to ensure homeostasis of emergent organismal "state variables", such as body temperature and organism size, through either elastic or plastic adaptation. Clearly, the conceptualization of a homeostat set to a desired setpoint disregards the architectural underpinnings of the organism's systems biology. Therefore, we conceptualize homeostasis as a dynamical—albeit stochastic—process, rather than as an end state (i.e., a setpoint). This view of organismal homeostasis and its centrality to the robust functioning of the organism naturally leads us to ask: *What quantitative principles ensure the robust and dynamical control of a stochastic yet homeostatic state variable of an organism?*

To address this question, here we turn to one of the simplest organisms—a bacterial cell—and one of its best-studied homeostatic state variables—cell size. Under optimal growth conditions, a single bacterial cell continuously grows and divides, rejuvenating itself and producing subsequent rounds of daughter cells through binary fission, all whilst maintaining a typical size, generation after generation, for a given environment. Yet, growth and division are inherently stochastic processes with significant fluctuations. How then does the typical size of an individual cell remain a tightly controlled variable (see Fig. 3)? Over successive generations, how are cells prevented from getting progressively larger and larger (or smaller and smaller), thus leading to runaway cell size distributions? The biological significance of cell size homeostasis is readily explained. If too large, the cell's surface-to-volume ratio interferes with the efficient import of essential molecules and the export of waste. If too small, the cell risks guillotining unsegregated chromosomes and running out of cytoplasmic resources as a result of small copy number fluctuations. Maintenance of the typical cell size through exquisite coupling between growth and division is thus essential for proper functioning of the organism.

Current models of cell size homeostasis, informed by a wealth of single-cell datasets involving several microorganisms, typically build on the "setpoint" perspective and focus on specific hypothesized paradigms, pithily described as sizer, timer, and adder [11–16]. These approaches use a deterministic lens to view specific intragenerational phenomenology, asking whether the size at division is purely independent ("sizer") or is a pure multiple ("timer") or pure additive ("adder") of the size at birth. This deterministic framework is then used as a quasi-deterministic heuristic to motivate the requirement that cell size homeostasis should be achieved intergenerationally, as shown in Fig. 1(A). The necessary condition is that the slope of the straight line that best fits the variation of size at division versus size at birth (as obtained from a scatter plot of the data pooled from many generations of many cells) must be less than the slope predicted by the timer model. Exhaustive efforts to parse the implications of these paradigms have established that data from related bacterial species inconveniently fall at various points along the continuum between specific paradigms [17] (although the preponderance of attention has focused on the adder paradigm and model bacterial systems [18–21]). An active debate centers around identification of which of these schemes provides the most accurate description of how "growth control" is actualized in different microorganisms, using theoretical extrapolations of intergenerational dynamics based on the observed intragenerational

phenomenology [14, 21, 22]. However, these schemes may be unequivocally distinguished only in the deterministic case; in reality, homeostasis is an inherently stochastic process (see Fig. 1). Our high-precision data directly and exhaustively establish (see Figs. 2, S1, S2, and S3) that multigenerational trains of sizes of individual cells deviate dramatically from the naïve predictions derived from these frameworks. Evidently, variations from the putative homeostatic "setpoint" are not only normal, but in fact an integral feature of the stochastic intergenerational homeostasis of an individual cell!

Results

To reimagine a framework for stochastic homeostasis, we need high-precision, multigenerational trains of data points from a large number of individual cells. A natural way to experimentally characterize this phenomenon is to track the size of a single bacterial cell growing in well-defined environmental conditions over a period of time much longer than the average generation, taking care to distinguish the original cell from its progeny after each division. However, rapid numbers growth of a cell population leads to exponential crowding of the region of interest in typical live-cell microscopy approaches [23], severely limiting the number of generations available for study. Although a number of ingenious approaches have been developed to address this challenge [24–26], potential artifacts such as cell–cell contacts and differential nutrient diffusion [27] reduce the precision in control over growth conditions that each cell experiences. Our SChemostat technology [23] addresses each of these concerns (see Methods section for details), and thus proves instrumental in generating the requisite high-precision multigenerational datasets of statistically identical, non-interacting *Caulobacter crescentus* cells. Using this technology, we previously observed remarkably precise intragenerational "emergent simplicities" or scaling laws in single-cell growth between successive division events. We established that the mean-rescaled distributions of cell sizes at different times since the previous division, and the mean-rescaled distributions of interdivision times from different conditions, collapse onto universal curves [28]. However, these intragenerational scaling laws do not provide the complete picture, as they do not guarantee intergenerational homeostasis. We therefore sought to characterize this process by characterizing the phenomena of stochastic growth and division over many generations without recourse to any *a priori* assumptions about the machinery responsible for homeostasis.

(A) Direct evidence of stochastic intergenerational homeostasis of individual bacterial cell sizes. Surprisingly, despite the extraordinary scrutiny this problem has received, direct evidence for stochastic intergenerational cell size homeostasis is not readily available in published works. What would constitute the necessary and sufficient condition to demonstrate that observed trains of intergenerational data are in fact consistent with cells in stochastic homeostasis? As one may intuit, constancy of the mean cell size, averaged over an asynchronous population in balanced growth, is a necessary condition. However, it alone is not sufficient. Stochastic intergenerational cell-size homeostasis also requires that the distribution of cell sizes at birth ("initial size distribution") itself be time-invariant. Here, we present individual-cell multigenerational SChemostat data from three different balanced growth conditions: cells grown in complex (undefined) media, minimal (defined) media, and dilute complex media. (See Methods and Supplementary Section for details.) By experimentally confirming both conditions (see Figs. 3, S4, S5) we provide direct evidence of stochastic intergenerational homeostasis of individual cells in these conditions.

(B) The question of memory: Is stochastic intergenerational cell size homeostasis achieved through elastic or plastic adaptation? By analyzing successive values of initial cell size, we find that the intergenerational cell size dynamics are Markovian. Briefly, given a specified generation's initial size (a_1), the distribution of the next generation's initial size (a_2) is completely determined and does not depend on the preceding generations' initial sizes (a_0, a_{-1}, and so on); see Figs. S6, S7, S8. (See the Methods section for the definition of the notation.) In other words, $P(a_n|a_{n-1}, a_{n-2}, a_{n-3}\ldots) = P(a_n|a_{n-1}) = P_1(a_n|a_{n-1})$ for any n under balanced growth conditions. This result is key to building the following intergenerational theoretical framework. The immediate implication is that, under balanced growth conditions, intergenerational cell size homeostasis is maintained through reflexive elastic adaptation. Surprisingly, under these conditions, cell size does not serve as a repository of intergenerational memory!

(C) Theoretical formulation of the stochastic intergenerational framework for cell size homeostasis. Using the key emergent simplicity that the intergenerational cell size dynamics are Markovian, the basic equation governing the multigenerational dynamics of cell sizes at birth is (see the Methods section and

[29] for details):

$$P_n(a_n|a_0) = \left[\int_{-\infty}^{\infty}\right]^{n-1}\left[P_1(a_n|a_{n-1})\prod_{j=1}^{n-1}\{P_1(a_j|a_{j-1})da_j\}\right]. \tag{1}$$

In this formulation, after a sufficient number of generations have elapsed ($n \gg 1$), homeostasis is achieved if $P_n(a_n|a_0)$ converges to the same well behaved distribution for all values of initial cell sizes, a_0. This is indeed true for our data in all three conditions (see Fig. 5).

(D) Emergent simplicity: A scaling law governing stochastic intergenerational homeostasis. We then extracted from data $P_f(a_f|a_i)$, the conditional probability distribution of the final size conditioned on the initial size within the same generation, and found a remarkable emergent simplicity (see Fig. 4). This value is independent of the value of the initial size:

$$P_f(a_f|a_i) = \frac{1}{\mu_f(a_i)}\Pi_f\left(\frac{a_f}{\mu_f(a_i)}\right). \tag{2}$$

In the preceding equation, Π_f is the mean rescaled distribution with unit mean and $\mu_f(a_i) = \langle a_f|a_i\rangle$ is the mean of the final area, a_f, as a function of the initial area, a_i. This observation holds for all three growth conditions reported here. This emergent simplicity simplifies our task of developing the theory of stochastic intergenerational homeostasis; instead of considering $P_f(a_f|a_i)$, which is generally a function of two variables, we can now work with two one-dimensional functions, Π_f and μ_f. Among these, $\mu_f(a_i)$ simply serves as a "calibration curve" for restoring the un-scaled distribution from the universal mean-rescaled distribution for a given growth condition. From data, $\mu_f(a_i)$ is well approximated by a straight line (see Fig. S10).

(E) The exact stochastic map governing intergenerational cell size dynamics and homeostasis is directly validated by fitting-free data–theory comparisons. Taken together, these two emergent simplicities—the Markovian nature of intergenerational cell size dynamics (Figs. S6, S7, S8) and the intergenerational scaling law (Eq. 2)—serve as starting points to motivate and develop a data-informed theoretical framework. Furthermore, the data reveal yet another emergent simplicity: the division ratio, r, defined as the ratio of the initial size in a given generation to the final size (size at division) in the previous generation, is independent of the final size in the previous generation (see S9, [29] and the Methods section for details). Thus, $P(r|a_f) = P(r)$ is independent of a_f; when combined with Eq. (2), this implies that the conditional distribution of the next generation's initial size, conditioned on the current generation's initial size, must also undergo a scaling collapse upon rescaling by the conditional mean:

$$P_1(a_{n+1}|a_n) = \frac{1}{\mu(a_n)}\Pi\left(\frac{a_{n+1}}{\mu(a_n)}\right). \tag{3}$$

Here, Π denotes the new mean-rescaled distribution (with unit mean) and $\mu(a_n) = \langle a_{n+1}|a_n\rangle$ the conditional mean of the initial size in the next generation, given the initial size in the current generation. These functions can be related to the corresponding quantities in Eq. (2): $\Pi(s) = \left\langle r^{-1}\Pi_f(s\langle r\rangle/r)\right\rangle_r\langle r\rangle$ and $\mu(a) = \langle r\rangle\mu_f(a)$, where $\langle r\rangle$ is the mean division ratio and $\langle\cdot\rangle_r$ denotes averaging over fluctuations of r. We see direct evidence of this intergeneration scaling of initial sizes for all conditions, see Fig. S9. In the remaining sections, we will use this form of the intergenerational scaling law.

Using this intergenerational scaling law and the Markovian framework in Eq. (1), we can predict the complete stochastic map for intergenerational cell size statistics of an individual cell in a given balanced growth condition, using as inputs the universal mean-rescaled distribution function, Π, and the calibration curve corresponding to the conditional mean, μ, for that growth condition. See [29], the Methods section, and Fig. 5 for comparison between theoretical predictions and data. Our fitting free predictions match our data remarkably well for all conditions. Thus, we have written down a data-validated fitting-free theoretical framework: the stochastic map governing stochastic intergenerational homeostasis!

In a companion paper, [29], we show that our theoretical framework also accurately predicts the stochastic intergenerational cell size dynamics of other species of bacteria, *E. coli* and *B. subtilis*, using published datasets available for these organisms. It is noteworthy that these bacteria, unlike *C. crescentus*, can undergo

multifork replication when conditions are favorable, and obey additional constraints [30] which may not be applicable to *C. crescentus*. Yet importantly, the cell size dynamics leading to stochastic intergenerational homeostasis in these organisms are also governed by the theoretical framework we report here.

(F) Stochasticity specifies conditions for homeostasis. As we have see above, the implication of the observed intergenerational scaling law is that it fully determines the stochastic map governing intergenerational homeostasis. Furthermore, it determines the general necessary and sufficient conditions for stochastic homeostasis, given the observed linear form of the conditional mean, $\mu(a) = \alpha a + \beta$, as we derive in the companion paper [29]. In that work, we provide a simple bound on the value of the slope of the conditional mean, α: its magnitude must be less than or equal to $1/s_{\max}$, where $s_{\max}$ is the maximum allowed value of the variable governed by the mean-rescaled probability distribution Π in Eq. (3). Since Π has unit mean, the presence of stochasticity implies that $s_{\max} > 1$; thus, the homeostasis condition $|\alpha| \leq 1/s_{\max}$ is a stronger bound than the prediction $|\alpha| < 1$ of the quasi-deterministic sizer–timer–adder paradigm [18, 31–33].

(G) Reconciling the sizer–timer–adder framework with stochastic intergenerational dynamics: single cells are not "average" cells The setpoint picture and the attendant sizer–timer–adder quasi-deterministic framework have served as useful heuristics, inspiring a plethora of publications on cell size homeostasis in different microorganisms. However, as is clear from the stochastic dynamic intergenerational homeostasis framework developed in this work, the quasi-deterministic picture is not directly applicable to any single representative cell. Nonetheless, our theoretical framework may be used to clarify under what (unrealistic) limit the quasi-deterministic picture can be recovered.

In our companion paper [29], we show that our intergenerational framework, combined with the linear nature of the conditional mean, $\mu(a) = \alpha a + \beta$, produces the following consequence: given a starting cell size that is not equal to the homeostatic mean size, the mean size of this cell in subsequent generations relaxes exponentially to the homeostatic mean size, with an exponential rate given by $\ln(1/|\alpha|)$. A consequence is that the correlation function C_{mn} of the cell sizes in generations m and n is also an exponential function with rate $\ln(1/|\alpha|)$ (see the Methods section for details):

$$C_{mn} \propto \alpha^{|m-n|} = e^{-|m-n|\ln(1/\alpha)}. \tag{4}$$

Fig. S10 C, F, I provides a comparison between the theoretical prediction above and the experimentally calculated correlation function, showing good agreement.

This mean-level behavior is reminiscent of the quasi-deterministic evolution of cell size with generation, where it is predicted to exponentially relax to the setpoint size with the same exponential rate, $\ln(1/|\alpha|)$ (Fig. 6). Thus, the quasi-deterministic picture describes an "average" cell and not a representative cell.

Discussions and concluding remarks

In this work, we have used the bacterial cell size homeostasis problem as a valuable case study to directly grapple with the inherently stochastic and dynamic nature of homeostasis in living systems. The typical approach to describe homeostasis starts from a deterministic point of view, most notably the sizer–timer–adder framework, then adds "noise on top" to construct ad hoc quasi-deterministic frameworks motivated by analytic or computational tractability, rather than empirical observation. Here we take the radically different path of retaining the fully stochastic aspect of the problem at every stage of its conceptualization and description. We overcame the seemingly intractable complexity of this approach with a unique integration of techniques. High-precision, high-throughput multigenerational single-cell trajectories provided data of sufficient quantity and precision to identify remarkable and unexpected emergent simplicities. Armed with these insights, we could write down a first-principles-based analytic theory that yielded spectacular fitting-free data–theory matches, thus reinforcing the validity of the conceptual framework developed here. Finally, we have shown how the appropriate deterministic reduction of our fully stochastic description can recapitulate the known heuristics of the popular sizer–timer–adder framework. The key insight is that the mythical "average cell" described by the deterministic limit fundamentally fails to capture the true behaviors of the typical individual cell that experiences stochastic homeostasis [34].

En route to reimagining a conceptual framework for homeostasis, we uncovered three notable emergent simplicities in our high-precision multigenerational cell sizes trajectories. First, the stochastic intergenerational cell size dynamics are memory-free, or Markovian; thus, cell size homeostasis is main-

tained via the passive, elastic adaptation scheme. Second, the mean-rescaled conditional distribution of size at division in a given generation, given size at birth in the same generation, undergoes a scaling collapse. Third, since the division ratio distribution is sufficiently independent of the size at division, the mean-rescaled conditional distribution of size at birth in a given generation, given size at birth in the previous generation, undergoes a scaling collapse. Taken together, these results specify the exact stochastic map governing stochastic intergenerational cell-size homeostasis, as borne out by compelling data–theory matches, with no fine-tuning parameters. Furthermore, they determine the necessary and sufficient condition for stochastic homeostasis, which is a stronger condition than that predicted by deterministic and quasi-deterministic frameworks like the sizer–timer–adder framework. We find that the conceptual framework and results presented here also accurately determine the dynamics of intergenerational homeostasis of other microorganisms for which data are available, based on our reanalysis of data previously published by other groups [29].

Thus, despite the long-standing criticism directed at the simplicity of Ashby's Homeostat, our work shows it to be a representative model for natural homeostasis in a living organism after all! Intergenerational cell size homeostasis urns out to be, like Ashby's Homeostat, an elastically adapting process. Perhaps this is the most startling and elegant simplicity of all. While excitement has been building around the general possibility that single cells may serve as useful arenas for exploring the phenomenology of learning without neurons [35–37], our work here shows that the bacterial cell size, under balanced growth conditions, is not a repository of cellular memory, and therefore cannot serve as a diffuse living brain with a capacity for learning on intergenerational timescales.

Our approach of identifying "top down" organism-level emergent simplicities complements the common atomistic view that understanding essentially complex phenomena in essentially complex systems, such as whole organisms, must focus on the dissection of genetic and signaling networks [38]. The results presented here transcend the minutiae of the condition-specific molecular networks implicated in growth control in distinct environmental conditions and organisms. The intergenerational scaling law holds across multiple balanced growth conditions, and across multiple bacterial species. However, the shape of the collapsed distribution changes from condition to condition. The mechanism is universal, but the specific instantiation depends on specifics of the balanced growth condition.

Where then is the controller for cell size homeostasis? Mechanistically, what specific coupling between the growth and division processes ensures that the intergenerational scaling law emerges? We explicate these architectural underpinnings in a complementary work [39]. The data presented here show early indications of a "precision–speed" tradeoff [40], encapsulated in the different shapes of the mean-rescaled curves from different growth conditions—narrower for the slower growth condition (defined minimal media) and broader for the faster growth condition (undefined complex media). What costs and benefits would determine the tradeoffs and optima in these contexts? An analogous precision–energy tradeoff is indicated in the observation that the slope, α, of the mean calibration curve, $\mu(a_i) = \alpha a_i + \beta$, is comparatively closer to the *upper* limit $1/s_{\max}$ set by our intergenerational framework, and not a lower value such as 0 which would correspond to perfect size control. These promising avenues for further investigation build on the insights here.

An accurate understanding of the general homeostasis problem may also provide valuable clues to address the problem of how living systems achieve sufficient dimensional reduction to ensure robust yet precise responses to varying environments. We can achieve a heuristic understanding of the dynamic range of the scales that must be transcended by considering how cells sense their environments. Microorganisms use two-component systems of which there are of the $\mathcal{O}(10\text{—}100)$ per cell [41]. Considering that each two-component system has a few output "states", combinatorially, the total readout from these sensors involves trillions of possible outcomes. Surely the coordinated response of a cell as a whole to changes in environment cannot involve computations to convert these outputs biochemically with trillions of entries! How then does the cell infer the whole-cell state from the trillions of microstates? One possibility is that homeostatic variables may serve as "state variables" of the cell under constant growth conditions, so that the cell can take a quick census of these few important variables and compute precisely how to respond and adapt when growth conditions change. Ongoing work on the complementary homeostatic variable identified in the previously reported intragenerational scaling laws—the instantaneous single-cell growth rate—may provide complementary clues to the dimension reduction mystery.

Methods

Experimental methods

The conditionally adhesive *C. crescentus* strain IB001 was introduced into a single-channel microfluidic device and cells were incubated for one hour in the presence of the vanillate inducer, which promotes adhesion. Growth medium was then infused through the channel at a constant flow rate of 10μL/min (Pump 11 Elite, Harvard Apparatus) to flush out non-adherent cells and ensure continuous delivery of nutrients and removal of waste. Growth medium consisted of complex medium (peptone-yeast extract; PYE), dilute PYE, or minimal growth medium with xylose as sole carbon source (M2X). A microscope (Nikon Ti Eclipse with perfect focus system) and motorized XY stage (Prior Scientific ProScan III) under computerized control (LabVIEW 8.6, National Instrument) were used to acquire phase-contrast images at a magnification of 250X (EMCCD: Andor iXon+; objective: Nikon Plan Fluor 100X oil objective plus 2.5X expander; lamp: Prior LED). The microfluidic device, growth media, and imaging apparatus were located inside a custom built acrylic microscope enclosure equilibrated to 30 C (temperature controller: CSC32J, Omega and heater fan: HGL419, Omega); this chamber was in turn located within a sealed environment with defined temperature and humidity for an additional level of environment control. Image analysis to extract single-cell growth trajectories was conducted using custom-built Python software.

Theoretical methods

Notation

We use a_i to denote generic initial size (size at birth) and a_f to denote final size (size at division); a_n (where n is distinct from i or f) is a random number that denotes the initial size in the nth generation; $\hat{a}_n$ is a random number that denotes the final size at the end of the nth generation; r is a random number that is the division ratio, the ratio of the initial size to the final size in the previous generation, defined using the relation $a_{n+1} = r\hat{a}_n$; $P(X)$ is the usual notation denoting the probability distribution of random variable X; $P(X|Y)$ denotes the conditional probability distribution of X conditioned on Y; $\langle X|Y\rangle$ denotes the conditional average of X conditioned on Y; $P_f(a_f|a_i)$ denotes the probability distribution of a_f conditioned on a_i within the same generation; $P_n(a|a_0)$ is the probability distribution of a_n at a conditioned on a_0, the initial size in generation 0, often referred to as the (arbitrarily chosen) "initial" generation; and $P_r(r)$ denotes the probability distribution of the division ratio r in any generation, while $P_r(r|a_f)$ is the distribution of r conditioned on the corresponding final size a_f.

Derivation of intergenerational framework

Since in balanced growth conditions the sequence of initial cell sizes $a_0 \to a_1 \to \ldots \to a_n$ occurs through a Markov process (i.e., is a Markov chain), the probability distribution of the final generation size, a_n, can be expressed as a convolution of conditional probabilities governing each step in the sequence:

$$P_n(a_n|a_0) = \iint P_1(a_n|a_{n-1})da_{n-1}P_1(a_{n-1}|a_{n-2})da_{n-2} \times \ldots \times P_1(a_2|a_1)da_1P_1(a_1|a_0). \tag{5}$$

This is the same as Eq. (1) in the main text.

Relating the functions Π and μ to Π_f and μ_f

We begin with the emergent simplicity encapsulated in Eq. (2), expressed for initial and final sizes in generation n:

$$P_f(\hat{a}_n|a_n) = \frac{1}{\mu_f(a_n)}\Pi_f\left(\frac{\hat{a}_n}{\mu_f(a_n)}\right). \tag{6}$$

The initial size in the next generation, a_{n+1}, can be found from the final size, $\hat{a}_n$, in generation n, using the division ratio r: $a_{n+1} = r\hat{a}_n$. Given that r is a random variable with distribution $P_r(r)$ that is independent of

$\hat{a}_n$, we can relate the mean of a_{n+1}, $\mu(a_n)$, to the mean of $\hat{a}_n$, $\mu_f(a_n)$, as follows:

$$\mu(a_n) = \langle\langle a_{n+1}\rangle\rangle_r = \langle\langle r\hat{a}_n\rangle\rangle_r = \langle r\rangle\langle\langle \hat{a}_n\rangle\rangle_r = \langle r\rangle\,\mu_f(a_n). \tag{7}$$

Note that there are two steps of averaging; the inner angular brackets average over possible growth-division processes at fixed r, whereas the outer angular brackets independently average over r). Meanwhile, the conditional probability distribution of a_{n+1} given a_n becomes:

$$\begin{aligned} P_1(a_{n+1}|a_n) &= \iint d\hat{a}_n dr P_r(r)\delta(a_{n+1} - r\hat{a}_n)P_f(\hat{a}_n|a_n) \\ &= \int dr P_r(r)\frac{1}{r}P_f\left(\frac{a_{n+1}}{r}|a_n\right). \end{aligned} \tag{8}$$

Herein, δ denotes the Dirac delta function. Using Eqs. (6) and Eq. (7),

$$\begin{aligned} P_1(a_{n+1}|a_n) &= \int dr P_r(r)\frac{1}{r}\frac{1}{\mu_f(a_n)}\Pi_f\left(\frac{a_{n+1}}{r\mu_f(a_n)}\right) = \left\langle \frac{\langle r\rangle}{r\mu(a_n)}\Pi_f\left(\frac{\langle r\rangle a_{n+1}}{r\mu(a_n)}\right)\right\rangle_r \\ &= \frac{\langle r\rangle}{\mu(a_n)}\left\langle \frac{1}{r}\Pi_f\left(\frac{\langle r\rangle}{r}\frac{a_{n+1}}{\mu(a_n)}\right)\right\rangle_r. \end{aligned} \tag{9}$$

We have thus arrived at the final intergenerational scaling form in the main text, Eq. (3), with the scaling function $\Pi(s)$ defined (setting $s = a_{n+1}/\mu(a_n)$ in the above) as:

$$\Pi(s) = \langle r\rangle\left\langle \frac{1}{r}\Pi_f\left(s\langle r\rangle/r\right)\right\rangle_r. \tag{10}$$

Deriving the correlation function, C_{mn}, from the mean

In balanced growth conditions with $\mu(a) = \alpha a + \beta$, when starting from an initial size a_0 (in generation 0) that is different from the homeostatic mean $\langle a\rangle_\infty$, the distributions of initial sizes in subsequent generations decay exponentially to the homeostatic mean with rate $\ln(1/\alpha)$:

$$\langle a_n - \langle a\rangle_\infty\rangle = (a_0 - \langle a\rangle_\infty)\,\alpha^n. \tag{11}$$

See [29] for details of the derivation. The angular brackets above denote a path average in a single cell. Since in balanced growth conditions generation 0 can be chosen arbitrarily, for $m > n$,

$$\langle a_m - \langle a\rangle_\infty\rangle = (a_n - \langle a\rangle_\infty)\,\alpha^{m-n}. \tag{12}$$

The correlation function C_{mn} requires us to perform both cell and population averages. Denoting the population average by $\langle\cdot\rangle_{\text{pop}}$ and assuming $m > n$,

$$\begin{aligned} C_{mn} &= \langle\langle(a_m - \langle a\rangle_\infty)((a_n - \langle a\rangle_\infty))\rangle\rangle_{\text{pop}} \\ &= \langle\langle(a_m - \langle a\rangle_\infty)((a_n - \langle a\rangle_\infty))\rangle\rangle_{\text{pop}} \\ &= \left\langle(a_n - \langle a\rangle_\infty)^2\right\rangle_{\text{pop}}\alpha^{m-n} = \text{Var}_\infty(a)\alpha^{m-n}. \end{aligned} \tag{13}$$

In the last step, $\text{Var}_\infty(a)$ is the generation-independent homeostatic variance of the size. When $m < n$, we exchange m and n in the expression, arriving at Eq. (4) in the main text.

Author Contributions

K.J. and S.I.-B. conceived of the research; K.J., R.R.B. and S.I.-B. designed the research; K.J. extracted the intergenerational scaling law from the data and performed data analysis under the guidance of S.I.-B.; K.J., R.R.B. and S.I.-B. developed the theoretical framework and performed analytic calculations; C.S.W. and S.I-.B. designed the experimental setup; C.S.W. and K.F.Z. actualized and refined the experimental pipeline under the guidance of S.I.-B.; C.S.W. and S.E. designed and developed the analysis pipeline with input from R.R.B. and S.I.-B.; C.S.W, K.F.Z., E.S., J.C. and S.I.-B. performed experiments; K.J., C.S.W., R.R.B. and S.I.-B. wrote the paper with input from all authors; S.I.-B. supervised the research.

Acknowledgements

We thank Purdue University Startup funds, Purdue Research Foundation, the Purdue College of Science Dean's Special Fund, and the Showalter Trust for financial support. K.J. and S.I.-B. acknowledge support from the Ross-Lynn Fellowship award. S.E. and S.I.-B thank Purdue's Data Mine Learning Community for computational resources. We are grateful to the Iyer-Biswas group members for insightful discussions and feedback. S.I.-B. thanks Daniel S. Fisher for useful questions.

References

1. Billman, G. E. Homeostasis: The Underappreciated and Far Too Often Ignored Central Organizing Principle of Physiology. *Frontiers in Physiology* **11** (2020).
2. Bernard, C. *Introduction à l'étude de la médecine expérimentale* **2** (JB Baillière, 1865).
3. Cannon, W. B. in *À Charles Richet: ses amis, ses collègues, ses élèves (in French)* (ed Pettit, A.) 91 (Les Éditions Médicales, Paris, 1926).
4. Cannon, W. B. *The Wisdom of the Body* (W.W. Norton & Company, Inc., New York, 1932).
5. Hardy, J. D. Control of heat loss and heat production in physiologic temperature regulation. *Harvey Lectures* **49,** 242–270 (1953–1954).
6. Wiener, N. *Cybernetics: or Control and Communication in the Animal and the Machine* (MIT Press, Cambridge, MA, 1948).
7. Kotas, M. E. & Medzhitov, R. Homeostasis, inflammation, and disease susceptibility. *Cell* **160,** 816–827 (2015).
8. Mukherjee, S. *The Song of the Cell: An Exploration of Medicine and the New Human* (Simon and Schuster, 2022).
9. Ashby, W. R. in *Design for a Brain* 100–121 (Springer, 1960).
10. Shannon, C. E. & Weaver, W. *The Mathematical Theory of Communication: 4. Print* (University of Illinois Press, 1969).
11. Spiesser, T. W., Müller, C., Schreiber, G., Krantz, M. & Klipp, E. Size homeostasis can be intrinsic to growing cell populations and explained without size sensing or signalling. *The FEBS journal* **279,** 4213–4230 (2012).
12. Deforet, M., van Ditmarsch, D. & Xavier, J. B. Cell-size homeostasis and the incremental rule in a bacterial pathogen. *Biophysical Journal* **109,** 521–528 (2015).
13. Taheri-Araghi, S. *et al.* Cell-size control and homeostasis in bacteria. *Current Biology* **25,** 385–391 (2015).
14. Sauls, J. T., Li, D. & Jun, S. Adder and a coarse-grained approach to cell size homeostasis in bacteria. *Current Opinion in Cell Biology* **38,** 38–44 (2016).
15. Logsdon, M. M. *et al.* A parallel adder coordinates mycobacterial cell-cycle progression and cell-size homeostasis in the context of asymmetric growth and organization. *Current Biology* **27,** 3367–3374 (2017).
16. Willis, L. & Huang, K. C. Sizing up the bacterial cell cycle. *Nature Reviews Microbiology* **15,** 606–620 (10 2017).
17. Jun, S. & Taheri-Araghi, S. Cell-size maintenance: universal strategy revealed. *Trends in Microbiology* **23,** 4–6 (2015).
18. Amir, A. Cell size regulation in bacteria. *Physical Review Letters* **112,** 208102 (2014).
19. Campos, M. *et al.* A constant size extension drives bacterial cell size homeostasis. *Cell* **159,** 1433–1446 (2014).
20. Lin, J. & Amir, A. The effects of stochasticity at the single-cell level and cell size control on the population growth. *Cell systems* **5,** 358–367 (2017).

21. Si, F. *et al.* Mechanistic origin of cell-size control and homeostasis in bacteria. *Current Biology* **29,** 1760–1770.e7 (2019).

22. Ghusinga, K. R., Vargas-Garcia, C. A. & Singh, A. A mechanistic stochastic framework for regulating bacterial cell division. *Scientific Reports* **6,** 30229 (2016).

23. Iyer-Biswas, S. *et al.* Scaling laws governing stochastic growth and division of single bacterial cells. *Proceedings of the National Academy of Sciences of the United States of America* **111,** 15912–15917 (2014).

24. Wang, P. *et al.* Robust growth of Escherichia coli. *Current Biology* **20,** 1099–1103 (2010).

25. Moffitt, J. R., Lee, J. B. & Cluzel, P. The single-cell chemostat: An agarose-based, microfluidic device for high-throughput, single-cell studies of bacteria and bacterial communities. *Lab on a Chip* **12,** 1487 (2012).

26. Norman, T. M., Lord, N. D., Paulsson, J. & Losick, R. Memory and modularity in cell-fate decision making. *Nature* **503,** 481–486 (2013).

27. Potvin-Trottier, L., Luro, S. & Paulsson, J. Microfluidics and single-cell microscopy to study stochastic processes in bacteria. *Current Opinion in Microbiology* **43,** 186–192 (2018).

28. Iyer-Biswas, S., Crooks, G. E., Scherer, N. F. & Dinner, A. R. Universality in stochastic exponential growth. *Physical Review Letters* **113** (2014).

29. Joshi, K., Biswas, R. R. & Iyer-Biswas, S. Intergenerational scaling law determines the precision kinematics of stochastic individual-cell-size homeostasis. *bioRxiv,* 2023.01.20.525000 (2023).

30. Scott, M. & Hwa, T. Bacterial growth laws and their applications. *Current opinion in biotechnology* **22,** 559–565 (2011).

31. Susman, L. *et al.* Individuality and slow dynamics in bacterial growth homeostasis. *Proceedings of the National Academy of Sciences* **115,** E5679–E5687 (2018).

32. Marshall, W. F. Cell geometry: how cells count and measure size. *Annual review of biophysics* **45,** 49–64 (2016).

33. Ginzberg, M. B., Kafri, R. & Kirschner, M. On being the right (cell) size. *Science* **348,** 1245075 (2015).

34. Sanders, S., Joshi, K., Levin, P. A. & Iyer-Biswas, S. Beyond the average: An updated framework for understanding the relationship between cell growth, DNA replication, and division in a bacterial system. *PLoS genetics* **19,** e1010505 (2023).

35. Rajan, D. *et al.* Single-cell analysis of habituation in Stentor coeruleus. *Current Biology* (2022).

36. Gunawardena, J. Learning Outside the Brain: Integrating Cognitive Science and Systems Biology. *Proceedings of the IEEE* **110,** 590–612 (2022).

37. Wright, C. S., Joshi, K. & Iyer-Biswas, S. Cellular learning: Habituation sans neurons in a unicellular organism. *Current Biology* **33,** R61–R63 (2023).

38. Hartwell, L. H., Hopfield, J. J., Leibler, S. & Murray, A. W. From molecular to modular cell biology. *Nature* **402,** C47–C52 (1999).

39. Joshi, K., Biswas, R. R. & Iyer-Biswas, S. Architectural underpinnings of stochastic intergenerational cell size homeostasis. *bioRxiv* (2023).

40. Lan, G., Sartori, P., Neumann, S., Sourjik, V. & Tu, Y. The energy–speed–accuracy trade-off in sensory adaptation. *Nature physics* **8,** 422–428 (2012).

41. Shapiro, L. & Losick, R. *Cell Biology of Bacteria* (Cold Spring Harbor Laboratory Press, 2011).

42. Jafarpour, F. *et al.* Bridging the timescales of single-cell and population dynamics. *Physical Review X* **8,** 021007 (2018).

43. Wright, C. S. *et al.* Intergenerational continuity of cell shape dynamics in Caulobacter crescentus. *Scientific Reports* **5,** 1–9 (2015).

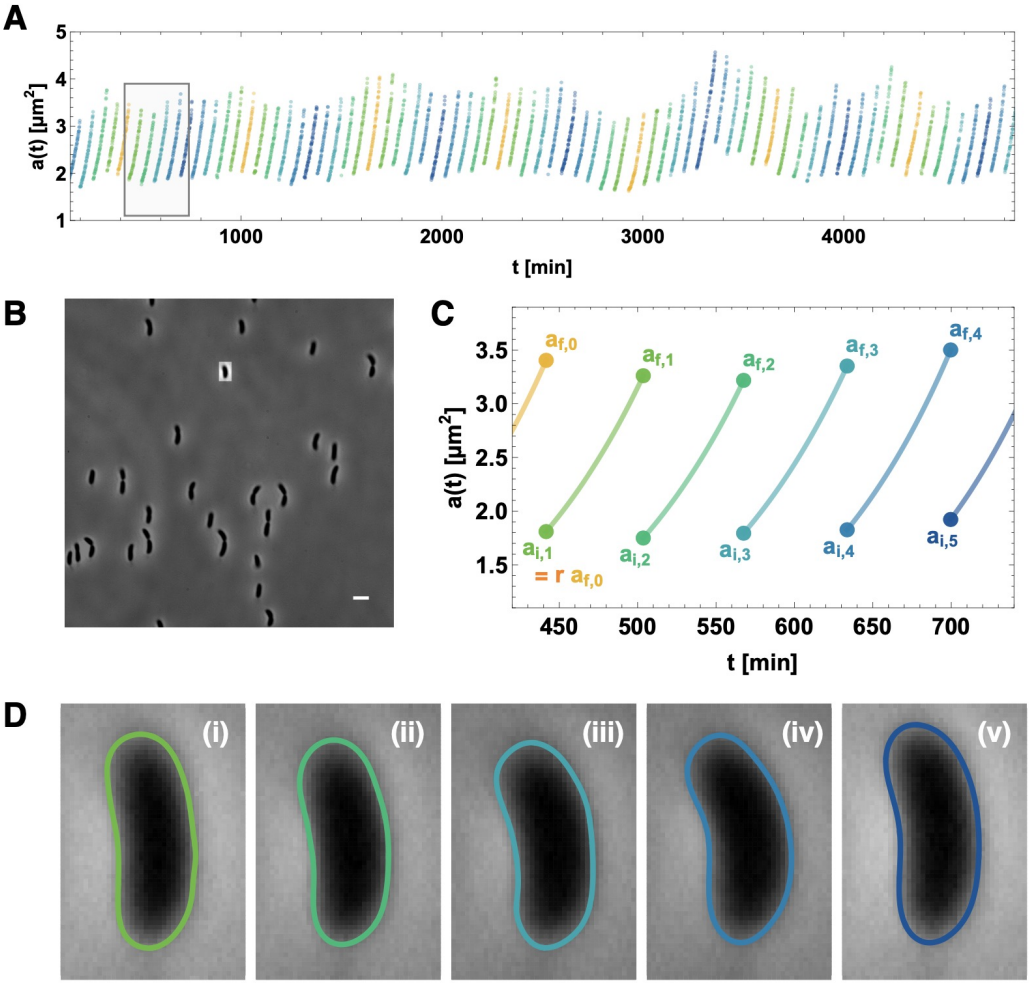

Figure 1: **Stochastic intergenerational cell size trajectories of individual bacterial cells.** **(A)** A typical individual *C. crescentus* stalked cell's intergenerational growth and division trajectory obtained using our SChemostat technology [23, 42], under time-invariant balanced growth conditions. Different colors indicate different generations of the cell. The local minima correspond to division events separating successive generations. The cell grows in size in the interdivision epochs. **(B)** Representative experimental field of view, with the cell corresponding to the trajectory in **A** highlighted. A typical experiment consists of tens of such fields of view, imaged tens of times between successive division events, with constant cell number and density for the duration of the experiment. Scale bar = 2 μm. **(C)** Exponential fits to growth trajectories of the generations highlighted by the box in **A**. In each generation the initial size ($a_{i,n}$, size at birth) and final size ($a_{f,n}$, size at division) are highlighted by the filled circles. r is the division ratio, which relates $a_{i,n}$ to $a_{f,n-1}$. **(D)** Cell boundary splines generated by our customized automated image analysis routines from the phase contrast images such as those shown in **B**. These boundaries are used to compute cell areas such as those shown in **A** with $\mathcal{O}(1\%)$ measurement precision, as detailed in [23, 43].

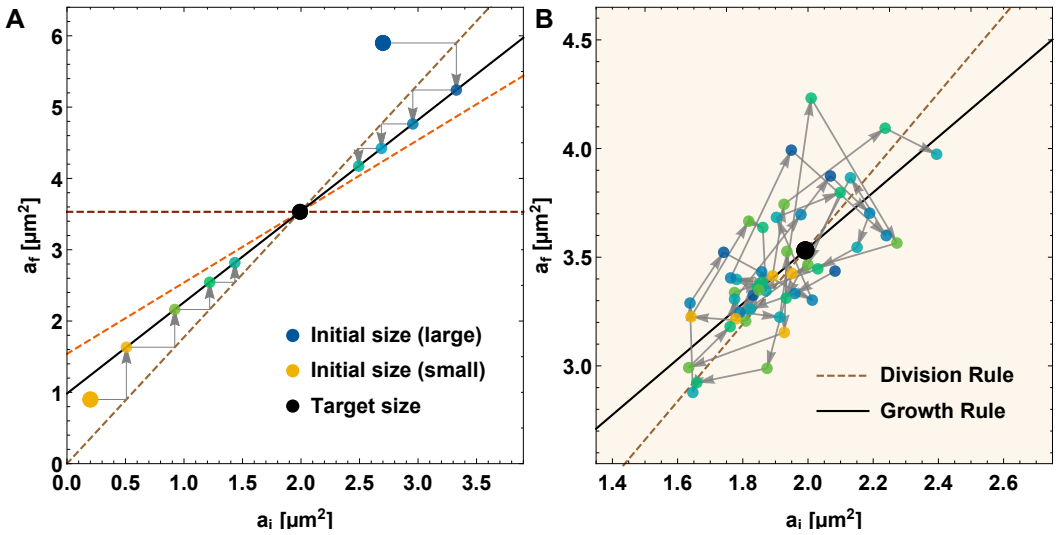

Figure 2: **Contrast between predictions from the sizer–timer–adder family of models and the inherently stochastic nature of intergenerational cell size dynamics as illustrated by our high-precision single-cell data. (A)** Geometric interpretation of the heuristic argument for intergenerational homeostasis in the quasi-deterministic sizer–timer–adder paradigms. The solid line, the "division rule", is $a_i = r a_f$. The dashed lines are "growth rules", $a_f = \alpha a_i + \beta$, whose slopes α are determined by the sizer (*maroon*, null slope), timer (*brown*, null intercept), and adder (*red*, unit slope) mechanisms. The "growth rule" allows the final size to be set by the initial size of the same generation. Thus, starting from an initial generation characterized by the coordinates of the large blue dot, the cell deterministically adjusts its size to exponentially relax to the target cell size set by the black point, the intersection between lines corresponding to the growth and division rules. **(B)** Representative trajectory calculated directly from our high-precision single-cell experimental observations. Evidently, **B** is dramatically different from **A**. Stochasticity is integral to intergenerational cell size homeostasis dynamics; there is no resemblance to the deterministic approach to a target size as suggested in **A**. Extensive sets of individual cell data as shown in **B** are given for all three balanced growth conditions in Figs. S1, S2, S3.

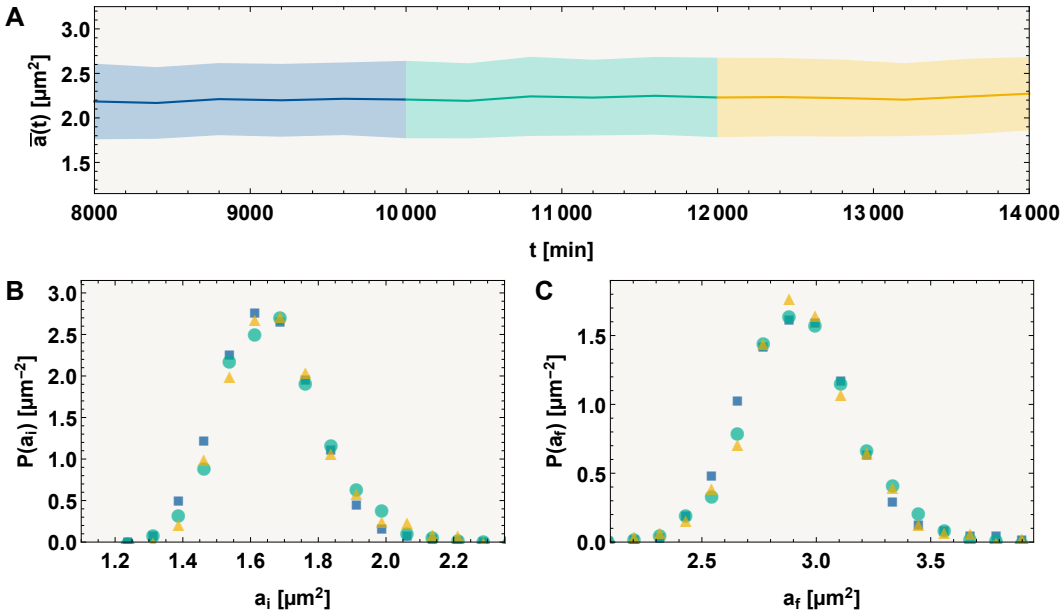

Figure 3: **Precision measurements establish that individual cells maintain stochastic intergenerational cell size homeostasis.** **(A)** The mean cell size averaged over an asynchronous population in balanced growth remains invariant when cell size homeostasis has been attained. The distributions of pooled **(B)** initial cell size (size at birth) and **(C)** final cell size (size at division) are plotted for cell generations within the three time bins in **A**, demarcated by the corresponding colors. These distributions are invariant, establishing that stochastic intergenerational homeostasis has been achieved and is sustained. Corresponding figures for individual cells in other balanced growth conditions are shown in Figs. S4, S5.

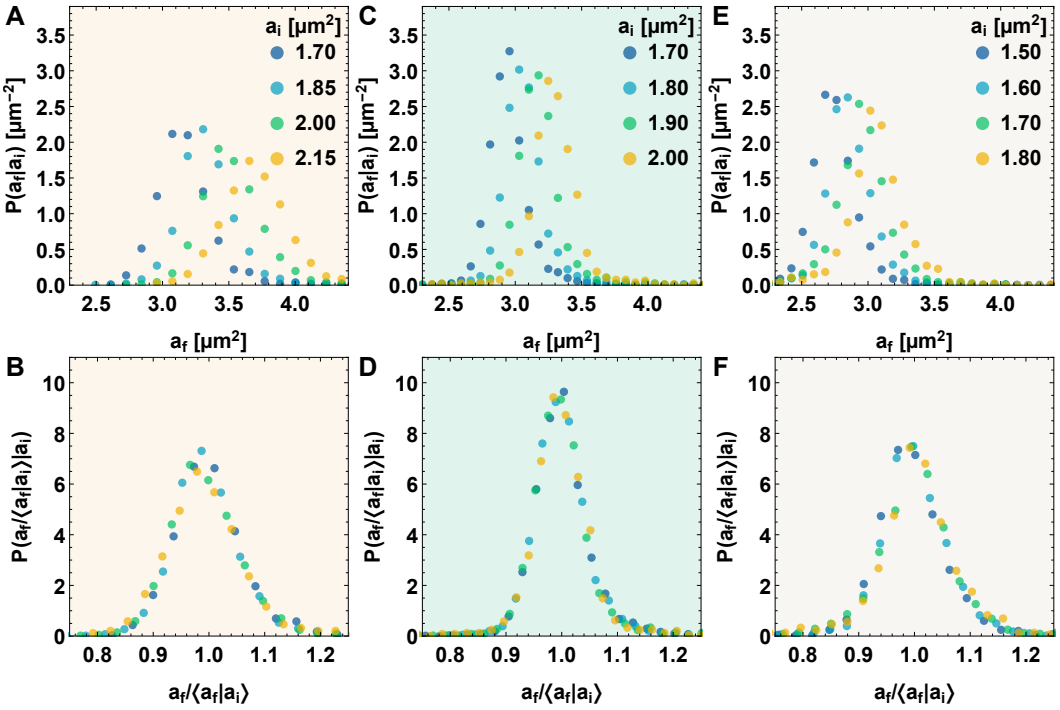

Figure 4: **Emergent simplicity: intergenerational scaling law governing stochastic individual cell size homeostasis.** The upper panels show the pre-division final size (a_f) distributions pooled by initial size values (with different a_i corresponding to different-colored points) within the same generation, $P_f(a_f|a_i)$, with the three figures corresponding to different growth media. These are converted to mean-rescaled distributions in the corresponding lower panels (same growth media = same background color; different a_i correspond to different-colored points as in the upper panels). Here, $\langle a_f|a_i\rangle = \mu_f(a_i)$ is the mean a_f for a given a_i. These mean-rescaled distributions are seen to be independent of initial size values, a_i, but can differ between different growth conditions. Thus, we have found an emergent simplicity: given a growth condition, the two-dimensional function $P_f(a_f|a_i)$ is constructed from two one-dimensional functions—the mean-rescaled distribution as in the lower-panel figures, and the a_i-dependent mean $\mu_f(a_i)$, which sets the calibration curve for how to "stretch" the a_i-independent lower-panel rescaled figures to recover the a_i-dependent upper-panel figures. **A, B**: complex growth media, **C, D**: minimal growth media, **E, F**: dilute complex growth media.

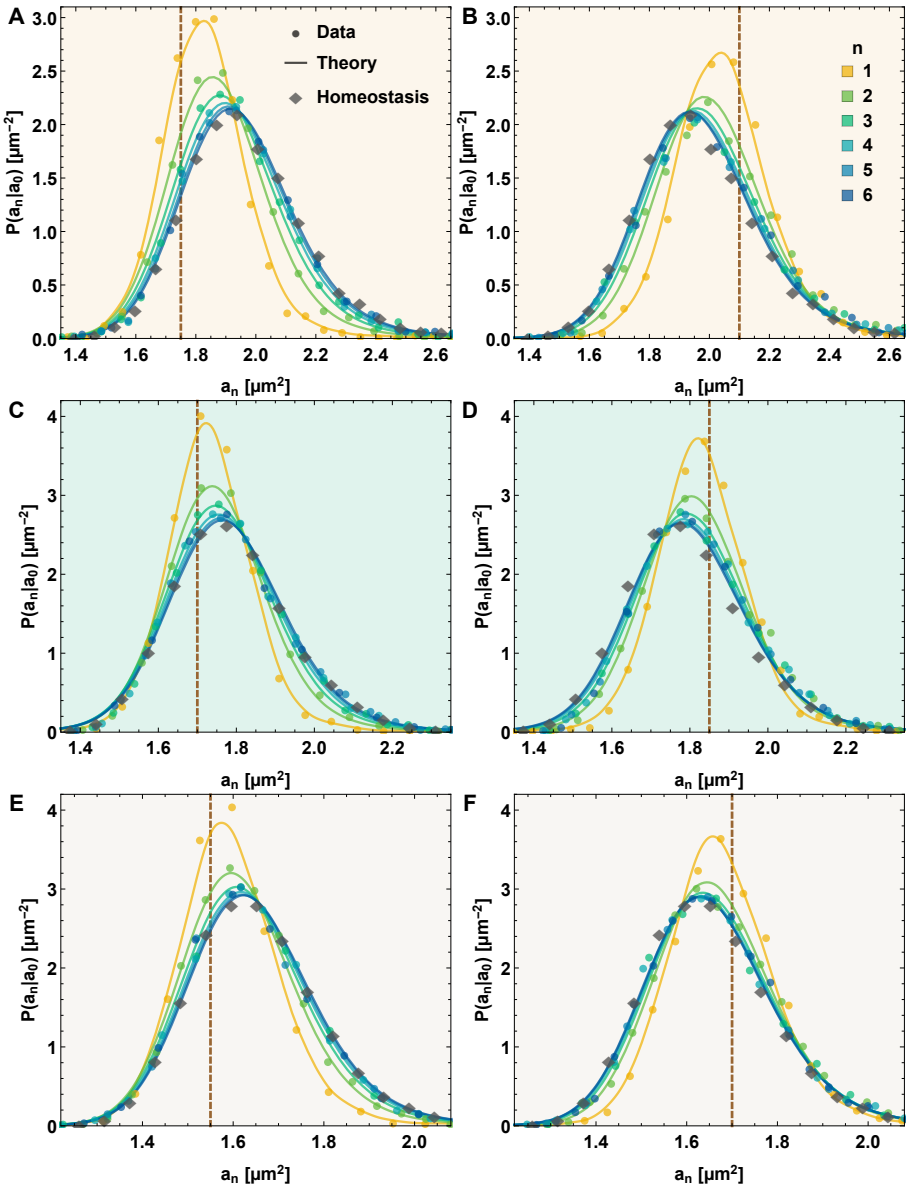

Figure 5: **Our theoretical framework accurately predicts, with no fitting parameters, the size-by-size intergenerational cell size dynamics leading to stochastic homeostasis.** Each panel shows the intergenerational evolution of the distribution of initial cell sizes, a_i, starting from a given initial size in the starting generation (location of dashed line). n denotes the generation number, with the starting generation labeled by $n = 0$. Each column corresponds to two different starting values of a_i for the same growth condition, while different rows correspond to different growth media, distinguished by different background colors. The points correspond to experimental data and the curves correspond to fitting-free predictions from our theoretical intergenerational framework, which takes as inputs the directly measured mean-rescaled distribution and mean calibration curve (discussed in Figs. S9, and S10 B, E, H).The compelling fitting-free data–theory match independently validates the emergent simplicities used as inputs for our theoretical framework: the Markovian nature of intergenerational cell size dynamics and a_i-independence of the mean-rescaled size distribution. **A, B**: complex growth media, **C, D**: minimal growth media, **E, F**: dilute complex growth media.

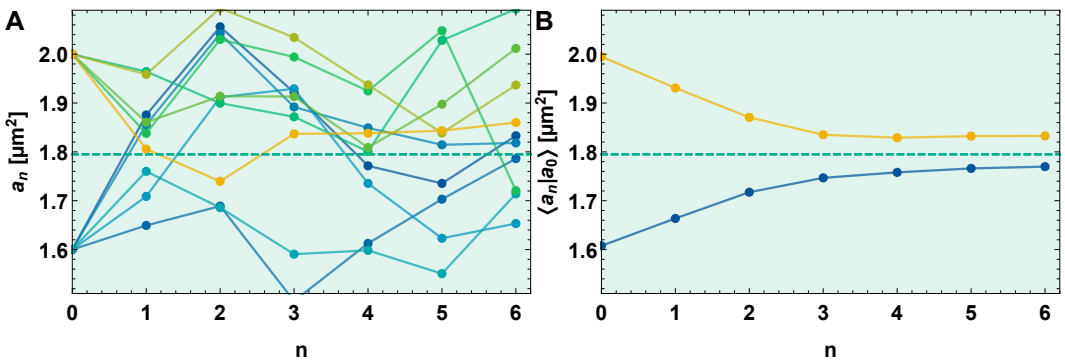

Figure 6: **Mythical "average" cell versus actual single cells' intergenerational attainment of homeostasis as observed in our experimental data.** Behavior of cells starting from given initial size. **(A)** Initial areas from five randomly selected trajectories over successive generations for cells starting from two different starting initial areas (1.6 and 2.0 μm^2, respectively). The dashed line represents the population mean of initial areas. **(B)** Mean initial areas across successive generations that start from the starting initial areas in **A**. Although the trajectories of individual cells do not follow a pattern discernible by eye, their mean converges to the population mean following the calibration curve of $\langle a_1|a_0\rangle$ in Fig. S10 E.

Supplementary Information

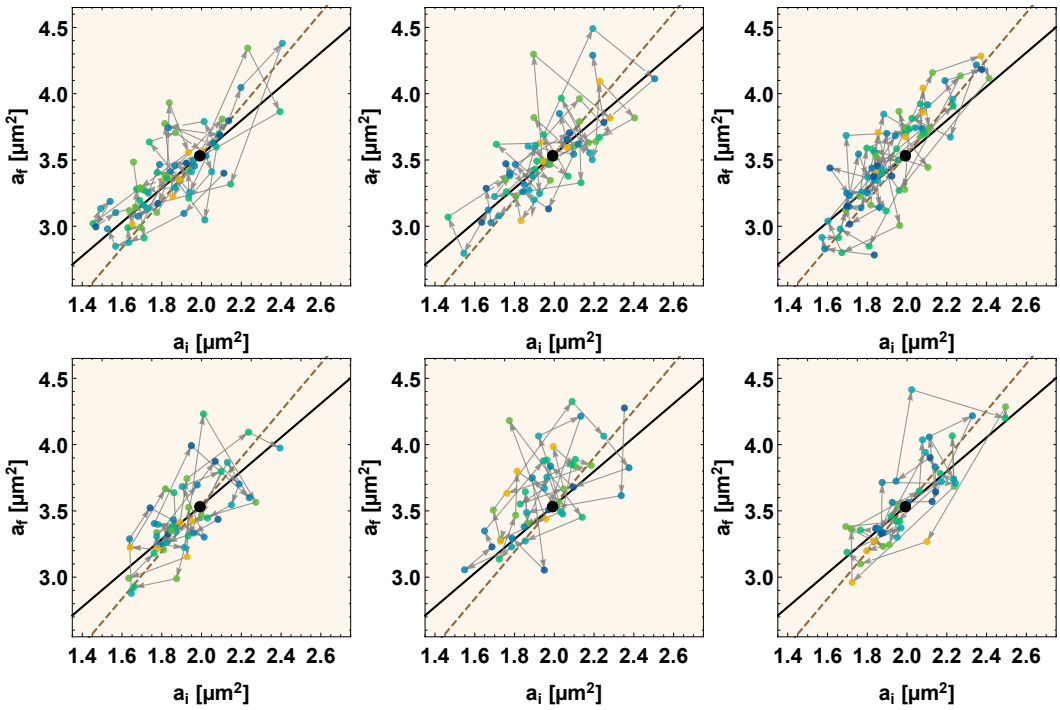

Supplementary Figure S1: **Representative single-cell intergenerational cell size trajectories calculated directly from our high-precision single-cell experimental observations in complex media.** Each data point is determined by the post-division (initial) and pre-division (final) cell sizes, a_i and a_f respectively, within the same generation. Successive generations are related by arrows. These are dramatically different from the prevailing quasi-deterministic adder-sizer-timer paradigm, see Fig. 2(A). Stochasticity is integral to intergenerational cell size homeostasis dynamics; there is no resemblance to the deterministic approach to a target size as suggested in Fig. 2(A). Also see data presented in Fig. 2(B). See also Figs. S2, S3 for representative single-cell trajectories in minimal and dilute complex media, respectively.

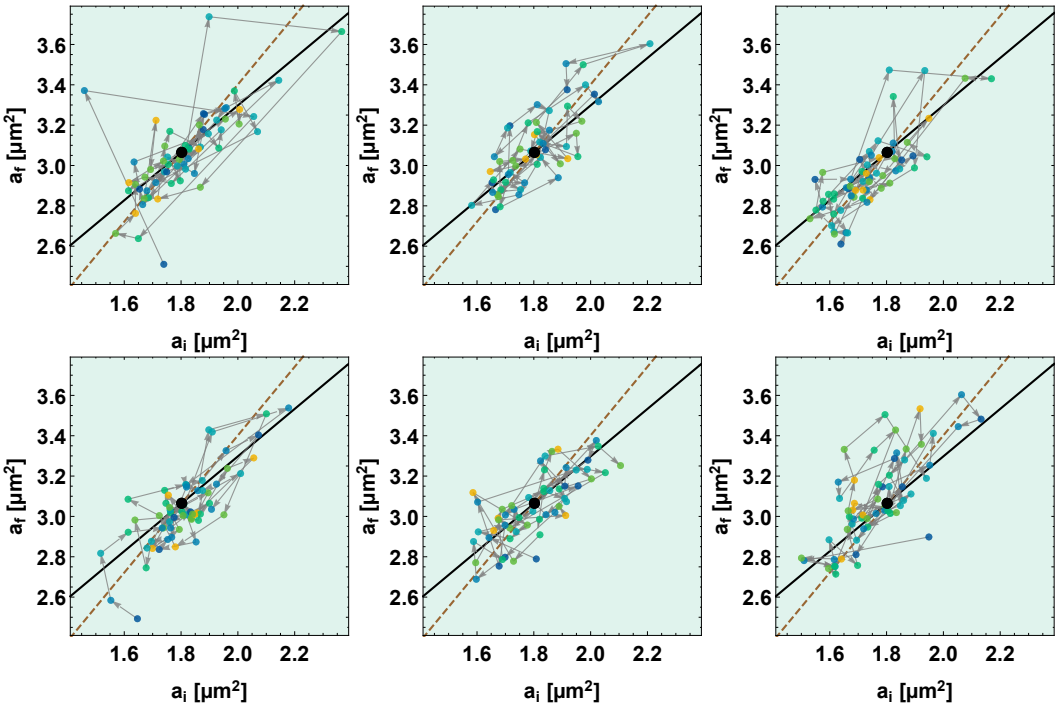

Supplementary Figure S2: **Representative single-cell intergenerational cell size trajectories calculated directly from our high-precision single-cell experimental observations in minimal media.** Each data point is determined by the post-division (initial) and pre-division (final) cell sizes, a_i and a_f respectively, within the same generation. Successive generations are related by arrows. These are dramatically different from the prevailing quasi-deterministic adder-sizer-timer paradigm, see Fig. 2(A). Stochasticity is integral to intergenerational cell size homeostasis dynamics; there is no resemblance to the deterministic approach to a target size as suggested in Fig. 2(A). Also see Figs. S1, S3 for representative single-cell trajectories in complex and dilute complex media, respectively.

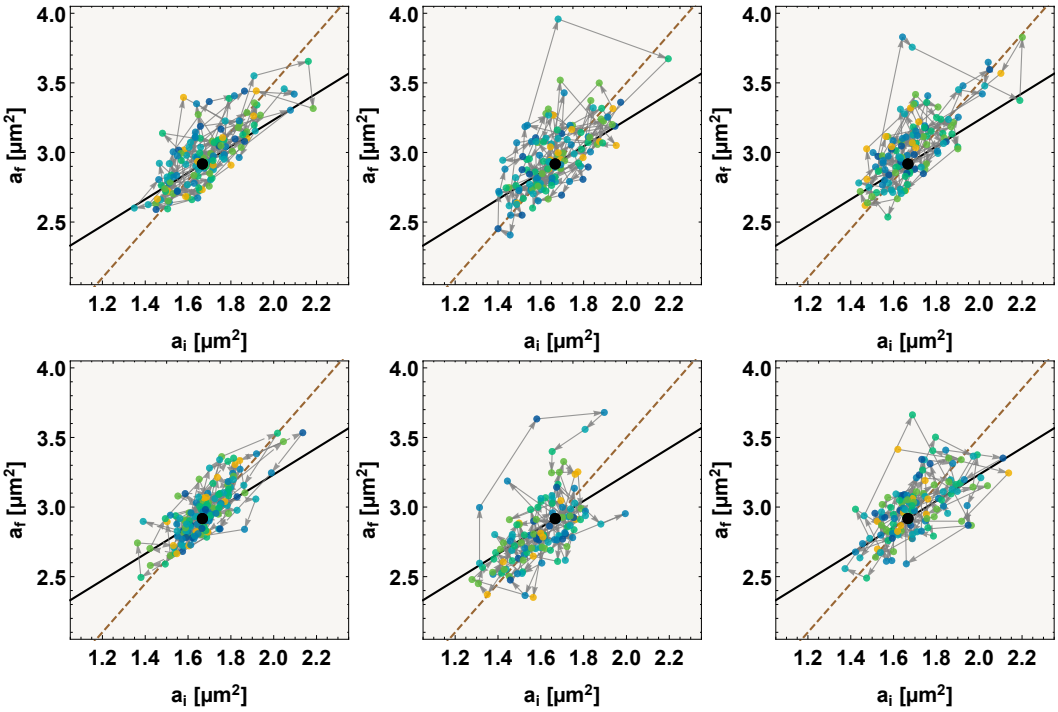

Supplementary Figure S3: **Representative single-cell intergenerational cell size trajectories calculated directly from our high-precision single-cell experimental observations in dilute complex media.** Each data point is determined by the post-division (initial) and pre-division (final) cell sizes, a_i and a_f respectively, within the same generation. Successive generations are related by arrows. These are dramatically different from the prevailing quasi-deterministic adder-sizer-timer paradigm, see Fig. 2(A). Stochasticity is integral to intergenerational cell size homeostasis dynamics; there is no resemblance to the deterministic approach to a target size as suggested in Fig. 2(A). Also see Figs. S1, S2 for representative single-cell trajectories in complex and minimal media, respectively.

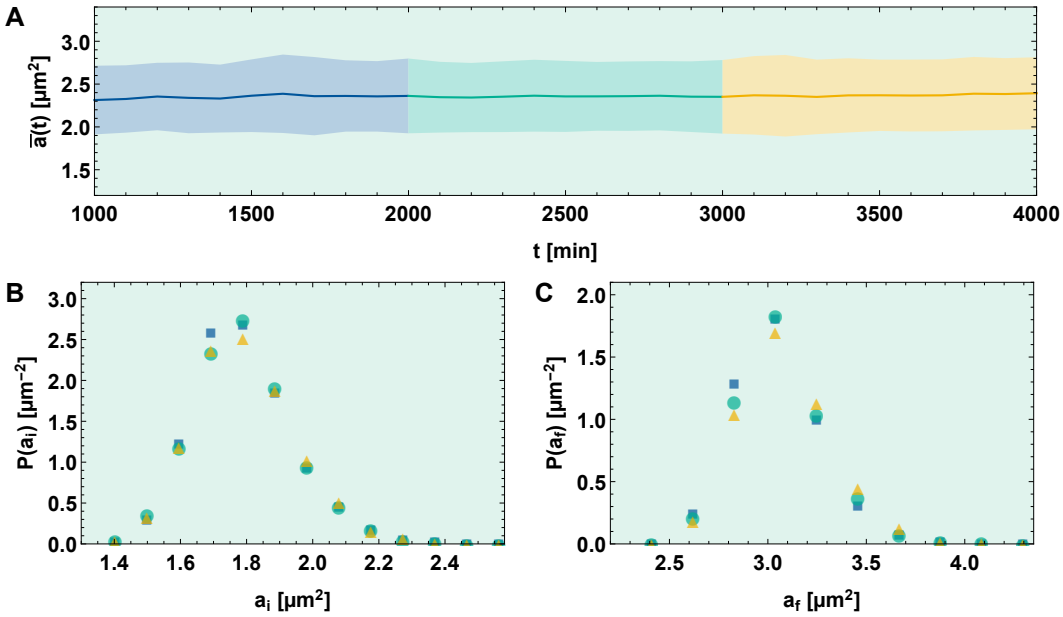

Supplementary Figure S4: **Precision measurements establish that individual cells maintain stochastic intergenerational cell size homeostasis, in minimal media.** (A) The mean cell size averaged over an asynchronous population in balanced growth remains invariant when cell size homeostasis has been attained. The distributions of pooled (B) initial cell size (size at birth) and (C) final cell size (size at division) are plotted for cell generations within the three time bins in A, demarcated by the corresponding colors. These distributions are invariant, establishing that stochastic intergenerational homeostasis has been achieved and is sustained. Corresponding figures for individual cells in other balanced growth conditions are shown in Figs. 3 and S5, corresponding to dilute complex and complex media respectively.

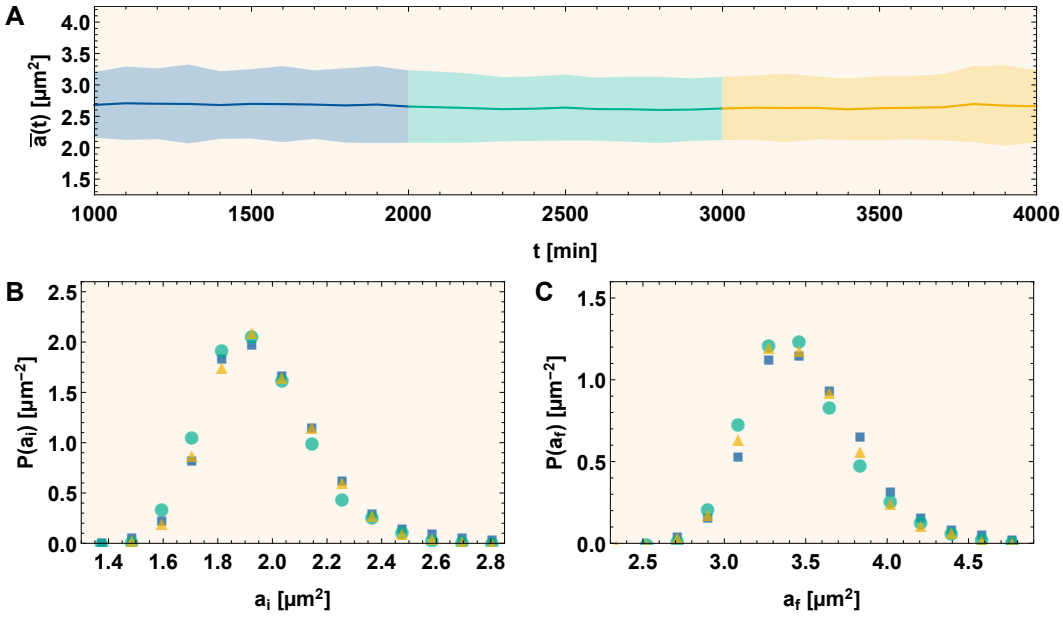

Supplementary Figure S5: **Precision measurements establish that individual cells maintain stochastic intergenerational cell size homeostasis in complex media.** (A) The mean cell size averaged over an asynchronous population in balanced growth remains invariant when cell size homeostasis has been attained. The distributions of pooled (B) initial cell size (size at birth) and (C) final cell size (size at division) are plotted for cell generations within the three time bins in A, demarcated by the corresponding colors. These distributions are invariant, establishing that stochastic intergenerational homeostasis has been achieved and is sustained. Corresponding figures for individual cells in other balanced growth conditions are shown in Figs. 3 and S4, corresponding to dilute complex and minimal media respectively.

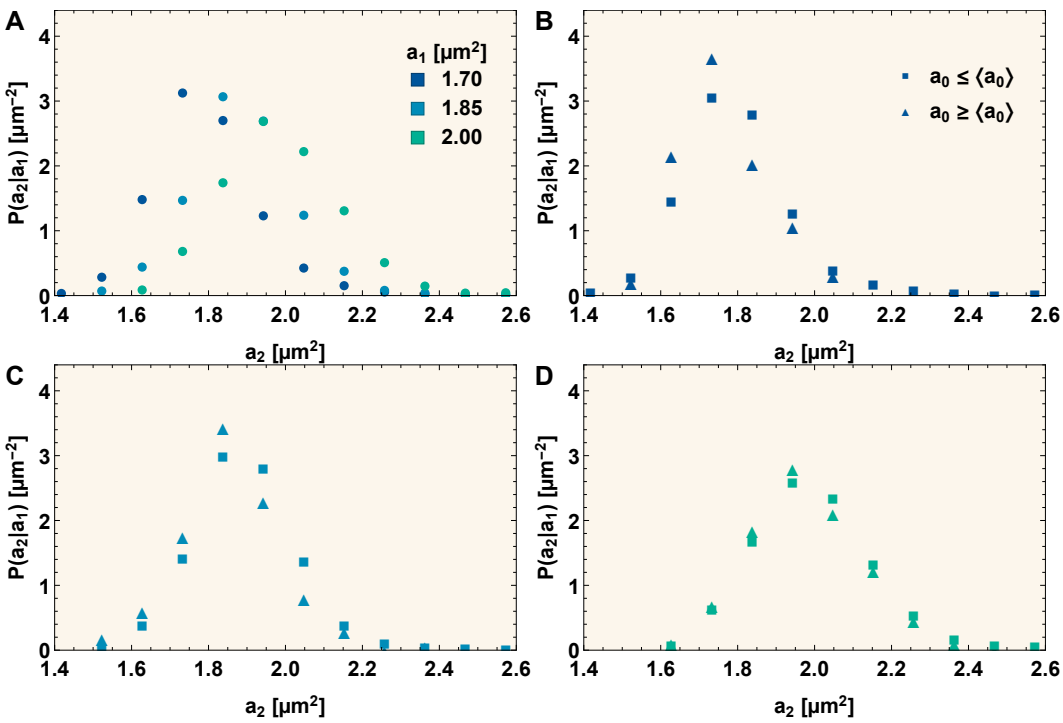

Supplementary Figure S6: **Evidence that the intergenerational cell size dynamics are Markovian; data taken from complex media balanced growth conditions.** (A) The distributions of subsequent generation's initial areas (a_2) given current generation's initial areas (a_1) are plotted for three different values of a_1s. (B-D) For each of the a1s in (A) (marked by different colors), the conditional distribution of subsequent generation's initial areas (a_2) given current generation's initial area (a_1) and given previous generation's initial area (a_0) less than or greater than the population mean initial area are plotted. The distributions overlap irrespective of whether a_0 was less than or greater than the population mean, indicating that a_2 does not depend on a_0 so long as the value a_1 is fixed. Thus, initial size dynamics are Markovian. See also Figs. S7 and S8 for data from minimal and dilute complex media respectively.

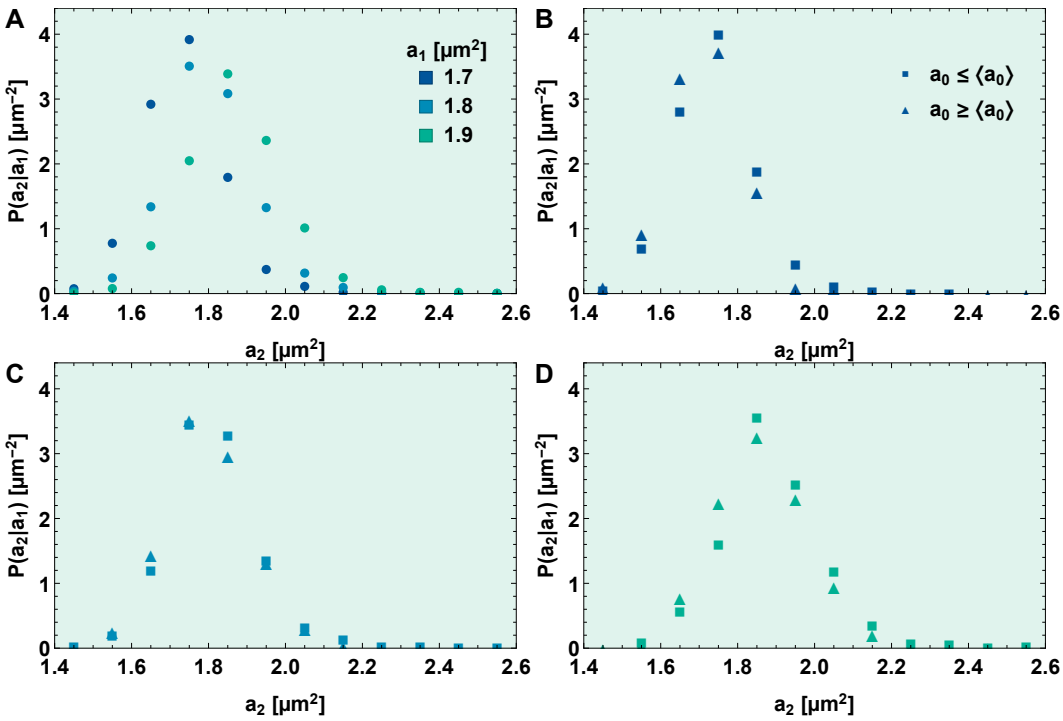

Supplementary Figure S7: **Evidence that the intergenerational cell size dynamics are Markovian; data taken from minimal media balanced growth conditions.** (A) The distributions of subsequent generation's initial areas (a_2) given current generation's initial areas (a_1) are plotted for three different values of a_1s. (B-D) For each of the a1s in (A) (marked by different colors), the conditional distribution of subsequent generation's initial areas (a_2) given current generation's initial area (a_1) and given previous generation's initial area (a_0) less than or greater than the population mean initial area are plotted. The distributions overlap irrespective of whether a_0 was less than or greater than the population mean, indicating that a_2 does not depend on a_0 so long as the value a_1 is fixed. Thus, initial size dynamics are Markovian. See also Figs. S6 and S8 for data from complex and dilute complex media respectively.

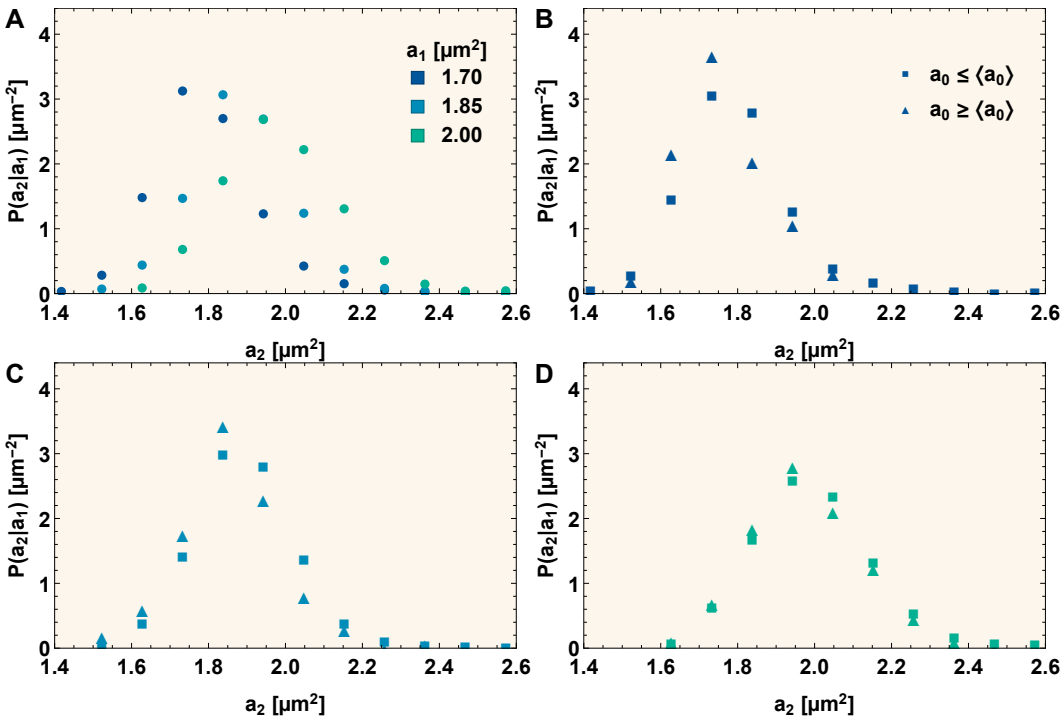

Supplementary Figure S8: **Evidence that the intergenerational cell size dynamics are Markovian; data taken from dilute complex media balanced growth conditions.** (A) The distributions of subsequent generation's initial areas (a_2) given current generation's initial areas (a_1) are plotted for three different values of a_1s. (B-D) For each of the a1s in (A) (marked by different colors), the conditional distribution of subsequent generation's initial areas (a_2) given current generation's initial area (a_1) and given previous generation's initial area (a_0) less than or greater than the population mean initial area are plotted. The distributions overlap irrespective of whether a_0 was less than or greater than the population mean, indicating that a_2 does not depend on a_0 so long as the value a_1 is fixed. Thus, initial size dynamics are Markovian. See also Figs. S6 and S7 for data from complex and minimal media respectively.

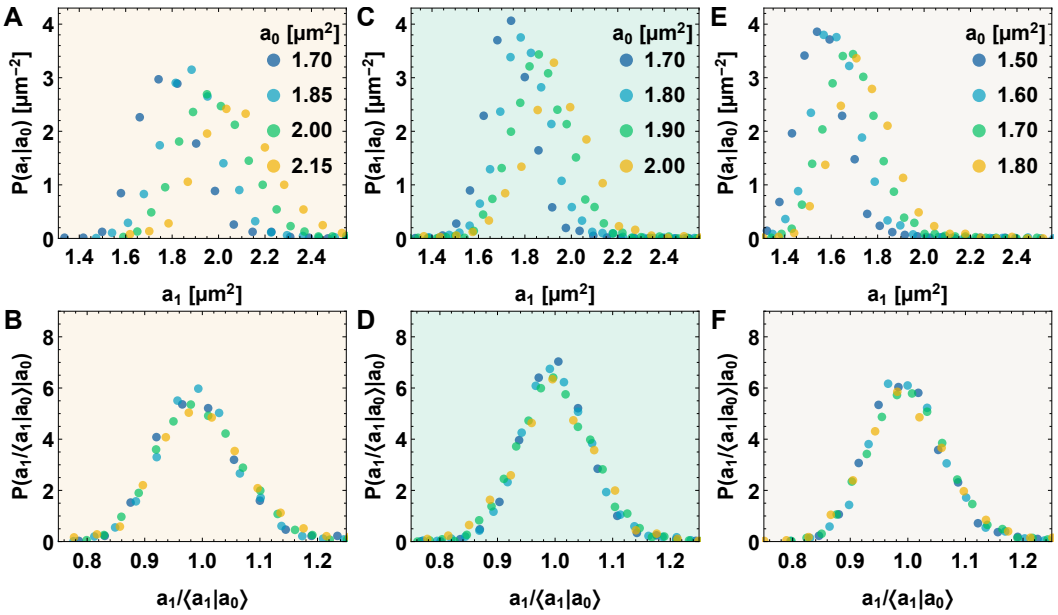

Supplementary Figure S9: **Intergenerational scaling: the mean rescaled next generation's initial size given this generation's undergoes a scaling collapse.** The upper panels show the next generation's initial size (a_1) distributions pooled by this generation's initial size values (with different a_0 corresponding to different-colored points), $P(a_1|a_0)$, with the three figures corresponding to different growth media. These are converted to mean-rescaled distributions in the corresponding lower panels (same growth media = same background color; different a_0 correspond to different-colored points as in the upper panels). Here, $\langle a_1|a_0\rangle = \mu(a_0)$ is the mean a_1 for a given a_0. These mean-rescaled distributions are seen to be independent of this generation's initial size values, a_0, but can differ between different growth conditions. Thus, given a growth condition, the two-dimensional function $P(a_1|a_0)$ is constructed from two one-dimensional functions—the mean-rescaled distribution as in the lower-panel figures, and the a_0-dependent mean $\mu(a_0)$, which sets the calibration curve for how to "stretch" the a_0-independent lower-panel rescaled figures to recover the a_0-dependent upper-panel figures. **A, B**: complex growth media, **C, D**: minimal growth media, **E, F**: dilute complex growth media.

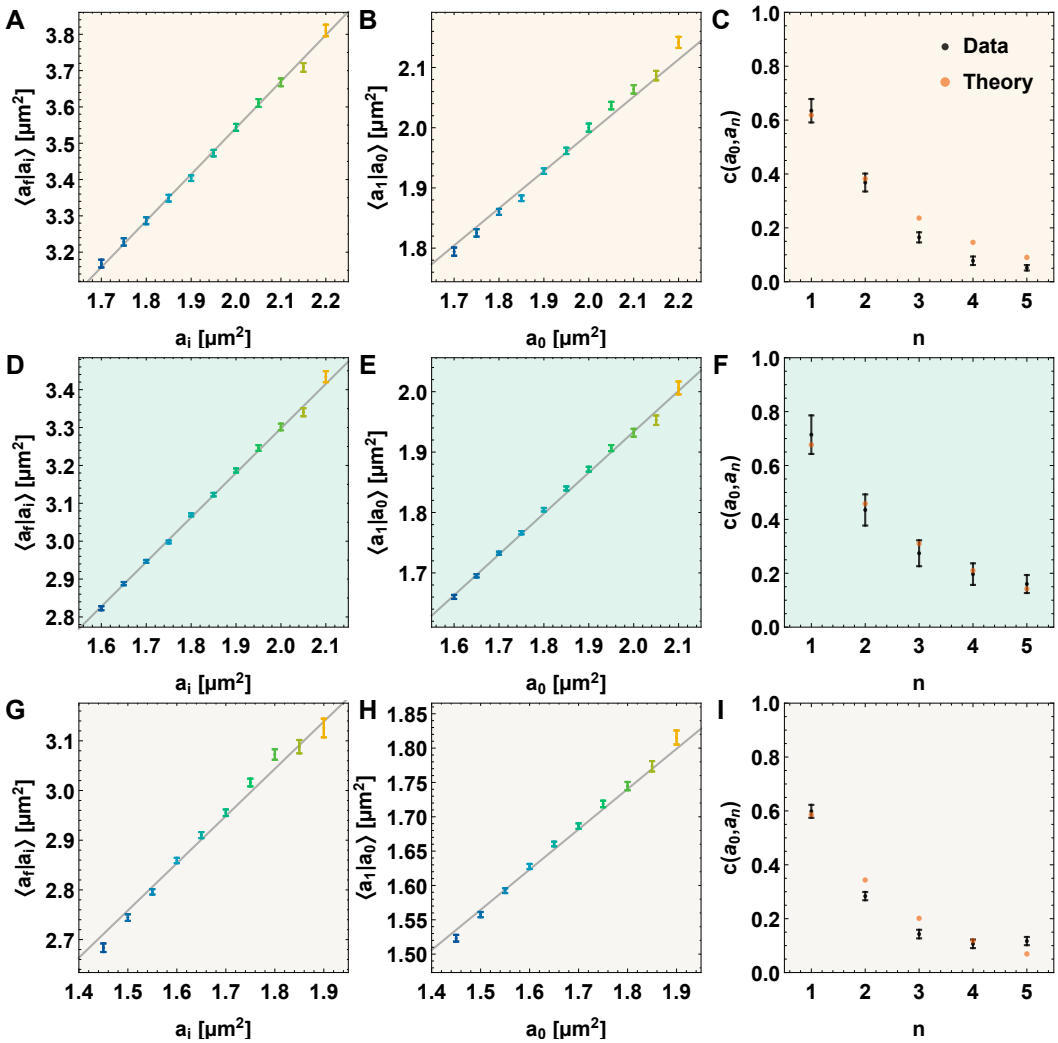

Supplementary Figure S10: **Calibration curves which restore the full distribution; generation-generation coefficient of correlations in cell sizes.** The left panels show the binned means of final areas plotted for a range of initial areas, along with the linear fit, with the three figures corresponding to different growth media. These calibration curves are used to restore the full conditional final size distributions conditional on initial size (Fig. 4 A, C, E) from the corresponding mean rescaled distributions (Fig. 4 B, D, F). The center panels show the binned means of next generation's initial areas plotted for a range of current generation's initial areas, along with the linear fit, with the three figures corresponding to different growth media (same growth media = same background color). These calibration curves are used to restore the full conditional next generation's initial size distributions conditional on this generation's initial size (Fig. S9 A, C, E) from the corresponding mean rescaled distributions (Fig. S9 B, D, F). The right panels show the coefficient of correlation between the initial areas in the initial (zeroth) generation and after n consecutive generations for different n. The correlations predicted by our fitting parameter-free theoretical framework (orange) closely match those measured from data (black). **A-C**: complex growth media, **D-F**: minimal growth media, **G-I**: dilute complex growth media.